Assessment of peak tsunami amplitude associated with a great earthquake occurring along the southernmost Ryukyu subduction zone for Taiwan region

Yu-Sheng Sun[1], Po-Fei Chen[1], Chien-Chih Chen[1], Ya-Ting Lee[1], Kuo-Fong Ma[1] and Tso-Ren Wu[2]

5 [1]Department of Earth Sciences, National Central University, Taoyuan City, Taiwan 320, R.O.C.
[2]Graduate Institute of Hydrological and Oceanic Sciences, National Central University, Taoyuan City, Taiwan 320, R.O.C.

Correspondence to: Yu-Sheng Sun (shengfantasy@gmail.com)

Abstract. The southernmost portion of the Ryukyu Trench closed to Taiwan island is a potential region to generate 7.5 to 8.7 tsunami earthquakes by shallow rupture. The fault model for this potential region dips 10° northward with rupture length

10 of 120 km and width of 70 km. The earthquake magnitude estimated by fault geometry is Mw 8.15 with 8.25 m average slip as a constrain of earthquake scenario. The heterogeneous slip distributions over rupture surface are generated by stochastic slip model, the slip spectrum with k-2 decay in wave number domain, and they are consistent with above identical seismic conditions. The results from tsunami simulation illustrate that the propagation of tsunami waves and the peak wave heights largely vary in response to the slip distribution. The wave phase changing is possible as the waves propagate, even under the

15 same seismic conditions. The tsunami energy path is not only following the bathymetry but also depending on slip distribution. The probabilistic distributions of peak tsunami amplitude calculated by 100 different slip patterns from 30 recording stations reveal the uncertainty decreases with distance from tsunami source. The highest wave amplitude for 30 recording points is 7.32 m at Hualien for 100 different slips. Comparing with stochastic slips, uniform slip distribution will be extremely underestimated, especially in near field. In general, uniform slip assumption only represents the average

20 phenomenon so that it will ignore possibility of tsunami wave. These results indicate that considering effect of heterogeneous slip distribution is necessary for assessing tsunami hazard and that can provide more information about tsunami uncertainty for a more comprehensive estimation.

1 Introduction

Almost all destructive tsunamis are generated by shallow earthquakes that occur at subduction zone. There are recently

25 destructive tsunami events: the 2004, Mw 9.1, Sumatra earthquake (Lay et al., 2005), the 2010, Mw 8.8, Chile earthquake (Lay et al., 2010; Fritz et al., 2011) and the 2011, Mw 9.0, Tohoku earthquake (Goda et al., 2015; Goda and Song, 2016) and all of them occurred at subduction zone. The island of Taiwan located at the convergent boundary between the Philippine Sea Plate and the Eurasian Plate is possibly threatened from tsunami. The convergence rate in this area is approximately 80-

85 mm/yr (Seno et al., 1993; Yu et al., 1997; Sella et al., 2002; Hsu et al., 2009; Hsu et al., 2012). Thus, earthquakes occur

frequently in and around Taiwan. The shallow earthquakes that occur in the Manila Trench to the south and the Ryukyu Trench to the northeast are particularly tsunamigenic Also, the earthquakes in southernmost Ryukyu Trench is more active than north Manila Trench (Wu et al., 2013). The most well-known historic tsunami events that have occurred in northeast Taiwan are the 1867 Keelung tsunami (Yu et al., 2016) and the 1771 Yaeyama (Japan) earthquake (M_w~8) (Nakamura,
5   2009a). The historic recording demonstrates that Taiwan island has the potential of tsunami threat. Furthermore, the 2011 Tohoku earthquake induced powerful tsunami that destroyed coastal areas and caused nuclear accidents (Mimura et al., 2011). There are four nuclear power plants along the coast on Taiwan island so that it is necessary to carefully estimate the tsunami hazard and compound disasters.

10   Probabilistic tsunami hazard analysis (PTHA) is a modification of probabilistic seismic hazard analysis (PSHA) (Cornell, 1968; SSHAC, 1997), and it is intended to forecast as comprehensively as possible the probability of tsunami hazards for a given region. Considering tsunamis triggered by earthquakes, the recurrence rates of earthquakes have typically been estimated using the Gutenberg–Richter relationship (Gutenberg and Richter, 1944) for a defined source region. The assessment of wave heights is one of the primary differences between PTHA and PSHA which assesses ground motion based
15   on empirical attenuation relationships. Given the wide distribution of global tsunamigenic earthquakes within seafloor regions at subduction zones, the tsunami records obtained from coastal gauges or/and ocean buoys are too sparse to assess the associated hazards comprehensively, and the recording time since their deployment is too short to enable study of the recurrence intervals of tsunamis/earthquakes. As a result, the probabilities of tsunami hazards are often assessed using empirical approaches or tsunami simulations. In tsunami scenario, the existing tsunami catalogue is limited so that the
20   simulation is an effective approach. Conventional tsunami simulation adopts simple source approximation and applies elastic dislocation theory to calculate the deformation of the seafloor surface assuming a uniform slip over entire fault surface (Okada, 1985; Okal, 1982). However, the complexity of earthquake ruptures plays a substantial role in tsunami generation. Conventional approaches are therefore unable to capture various features of short-wavelength tsunamis in the near field (Geist, 2002; Geist and Parsons, 2009). Previous studies that simulate tsunamis resulting from historical earthquakes around
25   Taiwan (Ma and Lee, 1997; Wu et al., 2008) using uniform slip models agree only with long-wavelength observations. For hazard mitigation, it is critical that the amplitudes of tsunamis are predicted along various coasts for a given earthquake as accurately as possible. To make such predictions, the effects of rupture complexity must be taken into consideration. Recent developments in PTHA have included the adoption of stochastic slip distributions of earthquakes to determine the overall probability of particular tsunami heights. (Geist and Parsons, 2006, 2009). That method can be able to quantify the variations
30   for a reasonable estimation in evaluating the probability of specified tsunami heights at individual locations that result from a specific fault.

In this study, we assess tsunami heights along the coasts of Taiwan that is caused by the potential tsunamigenic zone at the southernmost end of the Ryukyu subduction zone. This potential zone is close to Taiwan and at least ten earthquakes (M_w>7)

have occurred over the past 100 years (Hsu et al., 2012). The largest one is Mw 7.7 in 1920 (Theunissen et al., 2010). For this area, the plausible magnitude of greatest earthquake was determined to a range between 7.5 and 8.7 (M_w). The fault zone is bounded by the Longitudinal Valley Fault to the west and the Gagua Ridge to the east (Hsu et al., 2012). This defined fault geometry with rupture length and width was employed and earthquake with magnitude 8.15 is used in the tsunami

5 simulations. The stochastic slip model is invoked to describe the uncertainty of the rupture pattern over the fault plane to enable a more realistic assessment of tsunami probability.

2 Great earthquake scenario and tsunami simulation

2.1 Assessment of Seismic Parameters

10 The estimating magnitude of the maximum possible earthquake scenario is essential for the fundamental seismic condition of tsunami simulation. This scenario, potential rupture fault, proposed by Hsu et al. (2012) occurs along the southernmost Ryukyu trench with rupture length of 120 km, width of 70 km and dip of 10°. Kanamori and Anderson (1975) investigated the relation between rupture area and moment, which revealed that the most average stress drops ($\Delta\sigma$) between 10 to 100 bars. The average stress drops for the most interplate earthquakes are around 30 bars so that we set an average stress drop of

15 30 bars. According to the stress drop and seismic moment (M_0) relations in dip slip (Kanamori and Anderson, 1975),

$$M_0 = \frac{\pi(\lambda+2\mu)}{4(\lambda+\mu)}\Delta\sigma W^2 L \tag{1}$$

we can obtain the moment for this scenario under the average stress drop of 30 bars and with a definite rupture geometry. In Eq. (1), μ is rigidity and λ is the Lamè constant. Additionally, the seismic moment can be presented by rupture area and average slip as below:

20 $$M_0 = \mu A \overline{D} \tag{2}$$

The seismic moment, moreover, is dependent on rupture area (A) and average slip ($\overline{D}$) so that the average slip can be estimated by following Eq. (2) and it is 8.25 m. Then the seismic moment can be transformed magnitude M_w by (Hanks and Kanamori, 1979)

$$M_w = \left(\frac{\log M_0}{1.5}\right) - 10.73 \tag{3}$$

25 Therefore, the maximum possible earthquake is M_w 8.15.

2.2 Stochastic Slip Model

The rupture process of an earthquake is extremely complex. The seismic inversion results reveal the slip distribution of rupture is heterogeneous with temporal development. Using a simplified uniform slip distribution to simulate tsunami only captures the long-wavelength portion of the tsunami fields (Geist and Dmowska, 1999). In addition, the temporal description of the seismic rupture process can be ignored because the propagation velocity of the tsunami waves is substantially slower than the seismic rupture velocity (Dean and Dalrymple, 1991; Ma et al., 1991; Wang and Liu, 2006). Thus, for static slip distribution, Andrews (1980) showed that it is directly related to stress changes and decays following k^{-2} power law in the wavenumber domain.

$$\left| F_{s,t}\left[D_{x,y} \right] \right| \propto k^{-2} \tag{4}$$

where $D_{x,y}$ is the slip distribution, F is the 2D Fourier transform, $k = \sqrt{k_x^2 + k_y^2}$ is the wave number. k^{-2} power law illustrates slip distribution has self-similar characteristics and from the fractal perspective, this characteristic also can be demonstrated (Tsai, 1997). Herrero and Bernard (1994) based on self-similar introducing the k-square model which leads to the ω-square model (Aki, 1967). The slip spectrum follows k^{-2} decay beyond the corner frequency, k_c, which is proportional to $1/L_c$. The L_c depends on characteristic rupture dimension. Within the k_c, phase is held constant (Geist, 2002).

The heterogeneous slip distribution is proportional to k^{-2} and is similar to a fractional Brownian motion as a stochastic process (Tsai, 1997). The stochastic slip distribution can be described by convolution in Fourier domain,

$$D_{x,y} \propto F_{x,y}^{-1}\left[F_{s,t}\left[X_{x,y} \right] \times k^{-2} \right] \tag{5}$$

where $X_{x,y}$ is random variable for spatial distribution; moreover, it makes phase random. The random distribution, X, which is best described by a non-Gaussian distribution, especially by a Lèvy distribution, can be calculated by reversing Eq. (5) (Lavallée and Archuleta, 2003; Lavallée et al., 2006). Lèvy distribution has 4 parameters α, β, γ and μ_L.

$$\varphi(t) = \begin{cases} \exp\left(-\gamma^\alpha |t|^\alpha \left[1 + i\beta\, \text{sign}(t)\tan\frac{\pi\alpha}{2}\left(|\gamma t|^{1-\alpha} - 1 \right) \right] + i\mu_L t \right), & \alpha \neq 1 \\ \exp\left(-\gamma|t|\left[1 + i\beta\frac{2}{\pi}\text{sign}(t)(\ln|t| + \ln\gamma) \right] + i\mu_L t \right) & , \quad \alpha = 1 \end{cases} \tag{6}$$

The parameter α, $0<\alpha\leq2$, affects the falloff rate of PDF for the tail. The parameter β, $-1 \leq\beta\leq1$, controls the skewness of PDF. The parameter γ, $\gamma>0$, controls the width of PDF. The parameter μ_L, $-\infty<\mu_L<\infty$, is related to the location of PDF. Lèvy distribution is good to describe the distribution of random variable, X, from real earthquake events, which implies the slip distribution without self-similar characteristic has heavy tail behavior (Lavallée et al., 2006). From the experiments of generating stochastic slip distribution, the heavy tail behavior affects the intensity of extreme value (Lavallée et al., 2003).

The stochastic slip distribution is generated by 2D spatial random distribution with convoluting self-similar characteristic beyond the corner frequency, constraining by rupture dimension, in wavenumber domain. In this study, the potential rupture fault is divided into 5×5 km subfaults and the number of gird mesh is 24×14. The spatial random variable produced adopts Lèvy distribution (α=1.51, β=0.2, γ=28.3, μ_L=-0.9) which is the results from Lavallée et al (2006) as Figure 1a. In the

5 perspective of mathematical operation, the slip distribution in Eq. (5) is a kind of filtered random distribution. However, for consistency with the physical behavior over the rupture surface supposed by the results of inverse method, the truncation has to be applied to the Lèvy distribution to constrain the extreme slip value. The synthetic slip distribution (Fig. 1b) produced by spatial random distribution in Figure 1a is heterogeneous and its power spectrum obeys k-square model at high wavenumber (Fig. 1c). The average slip of this synthetic slip distribution is 8.25 m, which represents earthquake energy

10 keeping a constant as estimating above, and maximum slip is 31.02 m. The 100 different slip distributions are produced for tsunami simulation. They represent the uncertainty of results of complex rupture process. In 100 sets, the maximum slip range is between 20.17 to 37.97 m. Figure 1b and 1d is the pattern causing the maximum and minimum wave height at the recording station 26 (Hualien) (Fig. 2). Both patterns affecting the propagation will show at Sect. 3.1.

2.3 Numerical Tsunami Simulation

15 Figure 2 shows numerical model, recording stations and fault model. The potential rupture fault is divided into 5×5 km subfaults, and the stochastic slip distribution model is applied to determine the amount of discrete slip on each subfault. Vertical seafloor displacements caused by rupture slip are calculated using elastic dislocation theory (Okada, 1985). The Cornell Multigrid Coupled Tsunami Model (COMCOT) (Liu et al., 1995, 1995; Wang and Liu, 2005, 2006) is used to perform the tsunami simulations. COMCOT solves the linear or nonlinear shallow water equations for spherical or Cartesian

20 coordinates using the finite difference method. With the flexible nested grid system, it can properly exhibit both efficiency and accuracy from the near-coastal region to the far-field region. Two grid layers are used to simulate the propagation of tsunamis. The resolution of the outer layer is 4 minutes for the solution of the linear shallow water equation, and the resolution of the inner layer is 1 minute for the solution of the nonlinear form of the shallow water equation. Based on the positions of tidal gauges maintained by the Central Weather Bureau (CWB), 30 stations along the coasts of Taiwan and the

25 outlying islands are set up to record the wave heights of the simulated tsunami.

3 The effect of heterogeneous slip on the tsunamis

The stochastic slip model produces different slip distributions with the same fault geometry, average slip and a constant seismic moment. The model is used to describe the heterogeneous slip pattern of earthquake and to further examine its effect

30 on the tsunamis occurring at the southernmost end of the Ryukyu subduction zone adjacent to Taiwan. According to the previous sections, the maximum possible earthquake is determined to be M_w 8.15 with 8.25 m average slip. Furthermore, the

uniform slip distribution on the rupture plane is also used to simulate tsunami for discussing the different between uniform and heterogeneous slip on the tsunamis.

3.1 Initial water elevation and energy propagation

Using the Okada (1985) model calculates seafloor deformation assuming a homogeneous elastic structure and ignoring the process of gradual rupture. Figure 3a shows the initial water elevations produced by uniform slip distribution and Figure 3b is its maximum free-surface elevation during the propagation. Figure 3c and 3e are the initial water elevations produced by stochastic slip distributions (Fig. 1b and 1d). The initial water elevation by uniform slip is simple and smooth, but for the stochastic slip models are more complex and more heterogeneous. Nonuniform slip causes an apparent change in the wavelength distribution of the initial free-surface elevation (the potential energy distribution), which affects the path of energy propagation. In the uniform slip scenario, the maximum free-surface elevation pattern is clear and controlled by topography. However, many strong and seemingly chaotic paths of wave energy appear in the nonuniform scenarios, and the ocean surface field has more uncertainties in terms of flow. In Figure 3b, the maximum free-surface elevation mainly travels toward two places where the seafloor elevation becomes shallower, relative to the deep areas northeast of Taiwan as bathymetry in Fig. 2. Although the propagation by nonuniform slip distributions (Fig. 3d and 3f) also has the same characteristics, it is notable that the paths followed by the wave energy differ, which depends on the rupture pattern. At the northeast of Taiwan in Figure 3f, there is a strong wave path connecting the two higher elevation part. However, this behavior does not occur in Figure 3b and 3d. Besides that, at the footwall side, the maximum elevation of Figure 3d is higher than Figure 3f. In Figure 3b, the high elevation only appears along the coast at footwall side. These results indicate the wave energy variation depends on rupture pattern causing differences in wave paths and leads to totally different tsunami amplitudes.

3.2 Wave characteristic

There are 30 stations along the coasts for recording the motion of sea level. Relative to other stations, the station 25 (Shihti), 26 (Hualien) and 27 (Suao) are near the potential rupture fault, and they have high wave amplitude and enormous variation in the tsunami simulation of 100 different slip distributions so that the time series of wave heights at these stations are shown as an example (Fig. 4). The varied wavelength distribution of the initial free-surface elevation results in substantial phase changes and different wave heights. It's worth noting that the average of the disordered and chaotic time series produced by the 100 different slip distributions is almost identical to the results from the uniform case. This implies the uniform case simply represents an average result and it cannot represent all of the possible situations.

According to the statistical results from 100 different slip patterns (Table 1) for 30 stations, Hualien station has the maximum wave amplitude, 7.32 m, and its maximum wave amplitude interval is 1.87 to 7.32 m. It is the widest interval for any recording site and the standard deviation of this distribution is 1.024. These indicate that Hualien station has high uncertainty in this scenario setting. However, the maximum wave amplitudes from uniform slip are relatively lower than stochastic results. Following above lecture, we need to rethink about that the estimation of uniform slip case is available for hazard analysis or not, even only focusing on the maximum wave amplitude issue.

3.3 The peak tsunami amplitude probability

According to the results of our simulations, we calculated the probability of the peak/maximum tsunami amplitudes (PTA) at each recording station as shown in Figure 5 by histogram. In order to verify the representativeness of the PTA probability distributions, another 100 different slip distributions that have the same seismic parameters are subsequently simulated. In Figure 5, the PTA distributions, black lines, by additional 100 sets are similar to the results from original 100 sets slip distribution (the distribution of historgram). At 26 station, the PTA value produced by uniform slip, orange bar, is a little bit lower than the minimum ofPTA distributionby first set (Fig. 4 and Fig. 5), but it is within the range by second set. Even so, the PTA distribution by 100 times simulations is approximately reliable. This test also reinforces the reproducibility of our simulations and demonstrates that the number of simulations is roughly satisfactory for statistical analysis. Of course, the more slip distribution we use, the more comprehensive and stable the range we obtain.

In Figure 5, the PTA distributions at eastern Taiwan, red markers, are obviously higher than the western, blue markers, due to the specified location of the source of tsunami. The PTA produced by uniform slip are generally located in the middle of the PTA distributions. Both of the PTA values from uniform slip distribution and the values of the PTA from stochastic slip distribution models decrease with the distance from potential fault because of the attenuation of wave propagation (Fig. 5 is for all stations and Fig. 6 shows station 20 to 30 in the eastern Taiwan). However, some stations are not perfectly following this, for instance, station 17, 19 and 21. They are perhaps affected by coastal topography and energy channel. From Figure 3d, station 21 comparing with neighboring coast is exactly at the location where the energy gathers. In addition, the broad distributions frequently occur at promontories along the coastline and are caused by complex propagation path effects between the source region and the recording locations (Geist, 2002). There are many compound factors to affect the tsunami propagation and maximum wave height. Figure 6 presents the relation between distance and wave height and also shows the PTA distribution as Figure 5. On the footwall side, the station 20 and 22 are outer island. They do not face the energy path directly (Fig. 3f) so that the PTA distributions are lower than station 21 and 23; even though the distance from fault are similar. On the hanging wall, station 29 is far from coast comparing other stations because of real location of station and numerical grid setting so that the PTA distribution is lower than station 30 (Fig. 3b). The PTA distributions and their average

values roughly appear a linear decrease with distance except the near field, station 26 and 27. Moreover, the ranges of PTA distributions convergent with distance, too.

On the other hand, the near field, station 26 and 27, are directly affected by seafloor deformation so that the PTA by uniform slip are quite low. Although the seismic parameters have defined already in our experiment and been held constants, there exist an uncertainty for PTA rather than a constant value. The uniform case cannot provide it and the PTA could be underestimated. Results give specific PTA ranges, which are the wave height uncertainties for the scenario of the earthquakes from Ryukyu Trench. The PTA of uniform slip case are within the possible range. Therefore, it is necessary to consider the effect by heterogeneous slip distribution for a comprehensively assessing tsunami hazard.

4 Discussion

4.1 Tsunami

Most coast threatened by near-field tsunami is parallel the subduction zone like the coast of Chile, Japan and Indonesia. There are many tsunami event occurring these regions such as the 2010, Mw 8.8, Chile earthquake, the 2011, Mw 9.0, Tohoku earthquake, the 2004, Mw 9.1, Sumatra earthquake, and the 2010, Mw 8.1, Mentawai earthquake (Satake et al., 2013). However, the potential rupture fault in this lecture along the southernmost Ryukyu subduction zone is perpendicular to the coast of Taiwan island, which directly affects the first movement of wave. On the footwall, the first movement is up, but conversely, it is down. On the hanging wall, people perhaps have more time to leave seafront because the coastline backs from land to sea at first tsunami wave. The location related to fault position generally determines the first situation, that helps for making disaster prevention and evacuation program.

The PTA distributions in the near field are broad and narrow with distance increasing from potential fault. The local behavior of tsunami runup is dominated by slip pattern of rupture. As Geist (2002) and Ruiz et al. (2015) mentioned, the effects by heterogeneous slip is important and necessary to consider for the near field estimation. Moreover, the numerical results by Ruiz et al. (2015) indicate the minimum PTA from stochastic slip model almost coincides with uniform slip computed. Geist (2002) shows the average and extrema PTA calculated for 100 different slip distribution and compares with uniform result. The relation of uniform result, average and extrema PTA is similar with our study results. Additionally, Ruiz et al. (2015) suggested that in near field, PTA from uniform slip is closed to minimum PTA from distribution. In this study result, only few near field stations which PTA from uniform slip are closed to minimum PTA from distribution, but the most PTA from uniform slip model are at middle of PTA distributions or almost close the average values, specially far from

tsunami source (Table 1). The different feature of near field PTA could be caused by fault geometry, seabed topography affecting the path of tsunami propagation and so on. The uniform slip assumption will underestimate runup in the near field.

There are four nuclear power plants on the Taiwan island. According to the numerical results, we infer that the PTA mean value of NPP4 coastal area is around 2 to 3 m. This distribution may be wilder than other nuclear power plants due to the relative position of tsunami source. Moreover, NPP4 locates a bay with curved shape so that the extra magnification effect perhaps makes PTA higher. The NPP3 also has this condition and then the energy concentrates at this area (Fig 3b, 3d and 3f). For NPP1 and NPP2 coastal area, the PTA distributions roughly locate between 1 and 2 m. The coast of this two nuclear power plants is facing the tsunami current slightly so that its PTA should be higher than neighbor coast (Fig 3b, 3d and 3f). In general, under this scenario, the coast of NPP4 has largest threat. Although the NPP3 is far from this tsunami source, it roughly faces 1.5 m wave height on average and has ±0.5m uncertain range. However, the NPP3 is more close to Manila subduction zone which could be threatened by the tsunami from Manila Trench. The coast of NPP1 and NPP2 is relative safe and has less uncertainty for PTA.

The use of a heterogeneous slip pattern clearly delineates the range of possible waveforms and provides more information on latent uncertainties of wave height. The 95% confidence intervals for wave height from 100 sets present in each time series and provide us a specific range for the motion of sea level (Fig. 4). According to these time series, we are aware of the periods of tsunami runup and runoff and can prepare the supporting policies to reduce disaster. For example, a nuclear power plant has the trench of water intake from ocean for cooling reactor, and if the motion of sea level is too low to take the water, the temperature of reactor will be too high and then cause the nuclear disaster. Therefore, this issue is necessary to pay attention in Taiwan because there are four unclear power plants located near the coast.

4.2 Stochastic slip model

The results of tsunami simulations illustrate that the effect of the slip distribution on the rupture plane has a significant effect on wave propagation and wave height. The correctness of this slip distribution determines whether the wave height calculations represent a useful reference or not. Many factors influence synthetic slip distributions. For instance, the exponent of slip spectrum associates with roughness of slip distribution. Higher exponential value inhibits the power of high wavenumber and leads it smoother; conversely, lower value leads it rougher. In general, k-square model needs to be followed. Furthermore, interpolation has a tremendous effect for the exponent value becoming larger with grid size reducing (Tsai, 1997). However, the random spatial variability of the slip distribution is more critical. According to Lavallée and Archuleta (2003, 2006), we adopted the truncated non-Gaussian distribution as a spatial variability. Truncation limits the non-Gaussian distribution to a particular range. It causes the heavy-tailed characteristic of this distribution to become less pronounced or even disappear, as in a Gaussian distribution. The synthetic slip is a filtering process in mathematics so that

the heavy-tailed characteristic affects the extremum of slip distribution. The maximum slip will be greater as the truncated range increases. The maximum slip may exceed reasonable values as truncated range is too wide. Therefore, the parameters must be chosen carefully in order to match the observations acquired by inversion.

5 **5 Conclusion**

The maximum possible earthquake scenario is M_w 8.15 with average slip of 8.25 m in the southernmost portion of the Ryukyu Trench. The 100 slip distributions of the seismic rupture surface were generated by a stochastic slip model. The maximum slip range is between 20.17 to 37.97 m and the average slip all consists with 8.25 m. The heterogeneous slip induces variability in tsunami wave heights and the associated paths of propagation. The simulated results demonstrate that

10 rupture complexity has a significant influence on the near field for local tsunami. The PTA distribution provide a specific range for wave height and its occurring probability in this scenario. These distributions and their average values roughly appear a linear decrease with distance. The coast, which is very close tsunami source or even upon, is directly affected by rupture slip. Then, the range of PTA distribution will converge with distance increasing from tsunami source. In this study, Hualien station, which is upon the source, has the wildest PTA interval (1.87-7.32 m) and the highest wave amplitude. The

15 statistical summary reveals this station, whose standard deviation is 1.63 and larger than other stations, has the largest uncertainty. However, the PTA caused by the uniform slip distribution is only 1.63 m, which is much lower, even below average (3.36 m) in this station. It implies that a simplified earthquake source cannot completely represent tsunami amplitudes in reality. If we adopt uniform slip to assess tsunami hazard, it will be critically underestimated. The tsunami amplitudes, which have characteristically extreme variance, are imperative for assessing tsunami hazards and the quantitative

20 techniques is also important.

References

Aki, K.: Scaling law of seismic spectrum, J. Geophys. Res., 72, 1217-1231, 1967.

Andrews, D. J.: A stochastic fault model: 1. Static case, J. Geophys. Res. Solid Earth, 85, 3867-3877, 1980.

25 Cornell, C. A.: Engineering seismic risk analysis, Bull. Seismol. Soc. Am., 58, 1583-1606, 1968.

Dean, R. G. and Dalrymple, R. A.: Water wave mechanics for engineers and scientists, World Scientific Publishing Co., Inc., 1991.

Fritz, H. M., Petroff, C. M., Catalan, P. A., Cienfuegos, R., Winckler, P., Kalligeris, N., Weiss, R., Barrientos, S. E., Meneses, G., Valderas-Bermejo, C., Ebeling, C., Papadopoulos, A., Contreras, M., Almar, R., Dominguez, J. C., and

30 Synolakis, C. E.: Field Survey of the 27 February 2010 Chile Tsunami, Pure Appl. Geophys., 168, 1989-2010, 2011.

Geist, E. L.: Complex earthquake rupture and local tsunamis, J. Geophys. Res. Solid Earth, 107, 2002.

Geist, E. L. and Dmowska, R.: Local tsunamis and distributed slip at the source. In: Seismogenic and Tsunamigenic Processes in Shallow Subduction Zones, Springer, 1999.

Geist, E. L. and Parsons, T.: Probabilistic analysis of tsunami hazards, Nat. Hazards, 37, 277-314, 2006.

5   Geist, E. L. and Parsons, T.: Assessment of source probabilities for potential tsunamis affecting the US Atlantic coast, Mar. Geol., 264, 98-108, 2009.

Goda, K. and Song, J.: Uncertainty modeling and visualization for tsunami hazard and risk mapping: a case study for the 2011 Tohoku earthquake, Stoch Env Res Risk A, 30, 2271-2285, 2016.

Goda, K., Yasuda, T., Mori, N., and Mai, P. M.: Variability of tsunami inundation footprints considering stochastic scenarios

10   based on a single rupture model: Application to the 2011 Tohoku earthquake, J. Geophys. Res. Oceans, 120, 4552-4575, 2015.

Gutenberg, B. and Richter, C. F.: Frequency of earthquakes in California, Bull Seismol Soc Am, 34, 185-188, 1944.

Hanks, T. C. and Kanamori, H.: A moment magnitude scale, J. Geophys. Res, 84, 2348, 1979.

Herrero, A. and Bernard, P.: A Kinematic Self-Similar Rupture Process for Earthquakes, Bull. Seismol. Soc. Am., 84, 1216-

15   1228, 1994.

Hsu, Y. J., Ando, M., Yu, S. B., and Simons, M.: The potential for a great earthquake along the southernmost Ryukyu subduction zone, Geophys. Res. Lett., 39, 2012.

Hsu, Y. J., Yu, S. B., Simons, M., Kuo, L. C., and Chen, H. Y.: Interseismic crustal deformation in the Taiwan plate boundary zone revealed by GPS observations, seismicity, and earthquake focal mechanisms, Tectonophysics, 479, 4-18,

20   2009.

Kanamori, H. and Anderson, D. L.: Theoretical basis of some empirical relations in seismology, Bull. Seismol. Soc. Am., 65, 1073-1095, 1975.

Lavallée, D. and Archuleta, R. J.: Stochastic modeling of slip spatial complexities for the 1979 Imperial Valley, California, earthquake, Geophys. Res. Lett., 30, 2003.

25   Lavallée, D., Liu, P. C., and Archuleta, R. J.: Stochastic model of heterogeneity in earthquake slip spatial distributions, Geophys. J. Int., 165, 622-640, 2006.

Lay, T., Ammon, C., Kanamori, H., Koper, K., Sufri, O., and Hutko, A.: Teleseismic inversion for rupture process of the 27 February 2010 Chile (Mw 8.8) earthquake, Geophys. Res. Lett., 37, 2010.

Lay, T., Kanamori, H., Ammon, C. J., Nettles, M., Ward, S. N., Aster, R. C., Beck, S. L., Bilek, S. L., Brudzinski, M. R.,

30   Butler, R., DeShon, H. R., Ekstrom, G., Satake, K., and Sipkin, S.: The great Sumatra-Andaman earthquake of 26 December 2004, Science, 308, 1127-1133, 2005.

Liu, P. L. F., Cho, Y. S., Briggs, M. J., Kanoglu, U., and Synolakis, C. E.: Runup of Solitary Waves on a Circular Island, J. Fluid Mech., 302, 259-285, 1995.

Liu, P. L. F., Cho, Y. S., Yoon, S., and Seo, S.: Numerical simulations of the 1960 Chilean tsunami propagation and inundation at Hilo, Hawaii. In: Tsunami: Progress in prediction, disaster prevention and warning, Springer, 1995.

Ma, K. F. and Lee, M. F.: Simulation of historical tsunamis in the Taiwan region, Terr. Atmos. Ocean. Sci, 8, 13-30, 1997.

Ma, K. F., Satake, K., and Kanamori, H.: The origin of the tsunami excited by the 1989 Loma Prieta Earthquake—Faulting or slumping?, Geophys. Res. Lett., 18, 637-640, 1991.

Mimura, N., Yasuhara, K., Kawagoe, S., Yokoki, H., and Kazama, S.: Damage from the Great East Japan Earthquake and Tsunami-a quick report, Mitig Adapt Strat Gl, 16, 803-818, 2011.

Nakamura, M.: Fault model of the 1771 Yaeyama earthquake along the Ryukyu Trench estimated from the devastating tsunami, Geophys Res Lett, 36, 2009.

Okada, Y.: Surface deformation due to shear and tensile faults in a half-space, Bull. Seismol. Soc. Am., 75, 1135-1154, 1985.

Okal, E. A.: Mode-wave equivalence and other asymptotic problems in tsunami theory, Phys. Earth Planet. Inter., 30, 1-11, 1982.

Ruiz, J., Fuentes, M., Riquelme, S., Campos, J., and Cisternas, A.: Numerical simulation of tsunami runup in northern Chile based on non-uniform k^{-2} slip distributions, Nat. Hazards, 79, 1177-1198, 2015.

Satake, K., Nishimura, Y., Putra, P. S., Gusman, A. R., Sunendar, H., Fujii, Y., Tanioka, Y., Latief, H., and Yulianto, E.: Tsunami Source of the 2010 Mentawai, Indonesia Earthquake Inferred from Tsunami Field Survey and Waveform Modeling, Pure Appl. Geophys., 170, 1567-1582, 2013.

Sella, G. F., Dixon, T. H., and Mao, A. L.: REVEL: A model for Recent plate velocities from space geodesy, J. Geophys. Res. Solid Earth, 107, 2002.

Senior Seismic Hazard Analysis Committee (SSHAC): Recommendations for Probabilistic Seismic Hazard Analysis: Guidance on Uncertainty and Use of Experts. Main Report NUREG/CR-6372 UCRL-ID-122160 Vol. 1, U.S. Nuclear Regulatory Commission, pp 256, 1997

Seno, T., Stein, S., Gripp A. E.: A model for the motion of the Philippine Sea plate consistent with Nuvel-1 and geological data. J. Geophys. Res. Solid Earth, 98 17 941−17 948. doi:10.1029/93JB00782.

Theunissen, T., Font, Y., Lallemand, S., and Liang, W.-T.: The largest instrumentally recorded earthquake in Taiwan: revised location and magnitude, and tectonic significance of the 1920 event, Geophys. J. Int., 183, 1119-1133, 2010.

Tsai, C. C. P.: Slip, stress drop and ground motion of earthquakes: A view from the perspective of fractional Brownian motion, Pure Appl. Geophys., 149, 689-706, 1997.

Wang, X. M. and Liu, P. L. F.: A numerical investigation of Boumerdes-Zemmouri (Algeria) earthquake and tsunami, Comput. Model. Eng. Sci, 10, 171-183, 2005.

Wang, X. M. and Liu, P. L. F.: An analysis of 2004 Sumatra earthquake fault plane mechanisms and Indian Ocean tsunami, J. Hydraul. Res., 44, 147-154, 2006.

Wu, T. R., Chen, P. F., Tsai, W. T., and Chen, G. Y.: Numerical Study on Tsunamis Excited by 2006 Pingtung Earthquake Doublet, Terr. Atmos. Ocean. Sci., 19, 705-715, 2008.

Wu, Y. H., Chen, C. C., Turcotte, D. L., and Rundle, J. B.: Quantifying the seismicity on Taiwan, Geophys. J. Int., 194, 465-469, 2013.

Yu, N. T., Yen, J. Y., Chen, W. S., Yen, I. C., and Liu, J. H.: Geological records of western Pacific tsunamis in northern Taiwan: AD 1867 and earlier event deposits, Mar. Geol., 372, 1-16, 2016.

5   Yu, S. B., Chen, H. Y., and Kuo, L. C.: Velocity field of GPS stations in the Taiwan area, Tectonophysics, 274, 41-59, 1997.
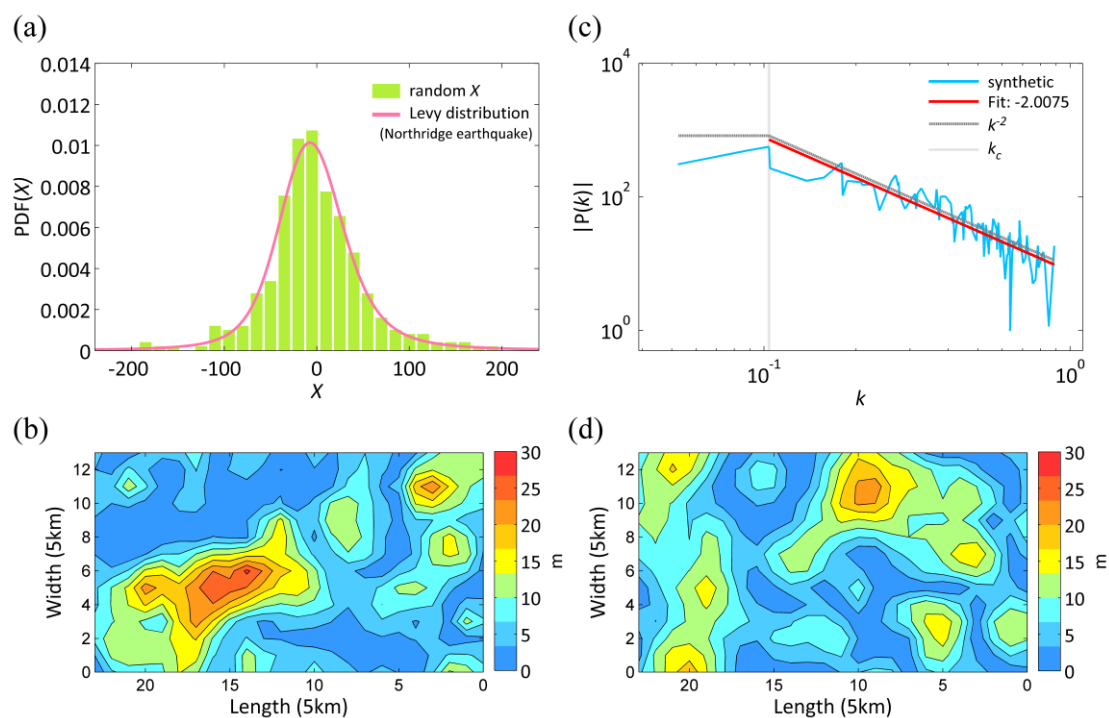
Fig. 1. (a) The spatial random variable: truncated Lèvy distribution. (b) A stochastic slip is generated from filtering the spatial random variable X, Fig. 1a. This slip pattern produces the highest maximum wave amplitude at Hualien station. (c) Slip spectrum
10 **is calculated from Fig. 1b. This slip spectrum decays with exponent of -2 and characteristic of corner frequency. It verifies that synthetic slip is identical with k-square model and condition of rupture dimension. (d) This stochastic slip distribution produces the lowest maximum wave amplitude at Hualien station.**
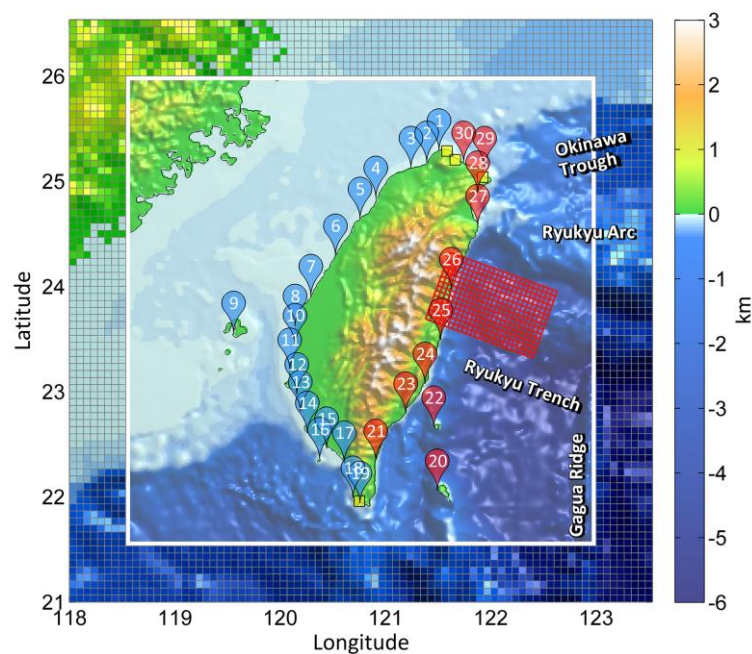
Fig. 2. The study area, recording stations and fault model. The resolution of the outer layer is 4 minutes, and the resolution of the inner layer is 1 minute. The red grid denotes the potential fault area (5×5 km). Pins represent 30 tidal gauges of the CWB. The red and blue colors indicate stations on the east or west sides of Taiwan, respectively. Yellow squares represent nuclear power plants.
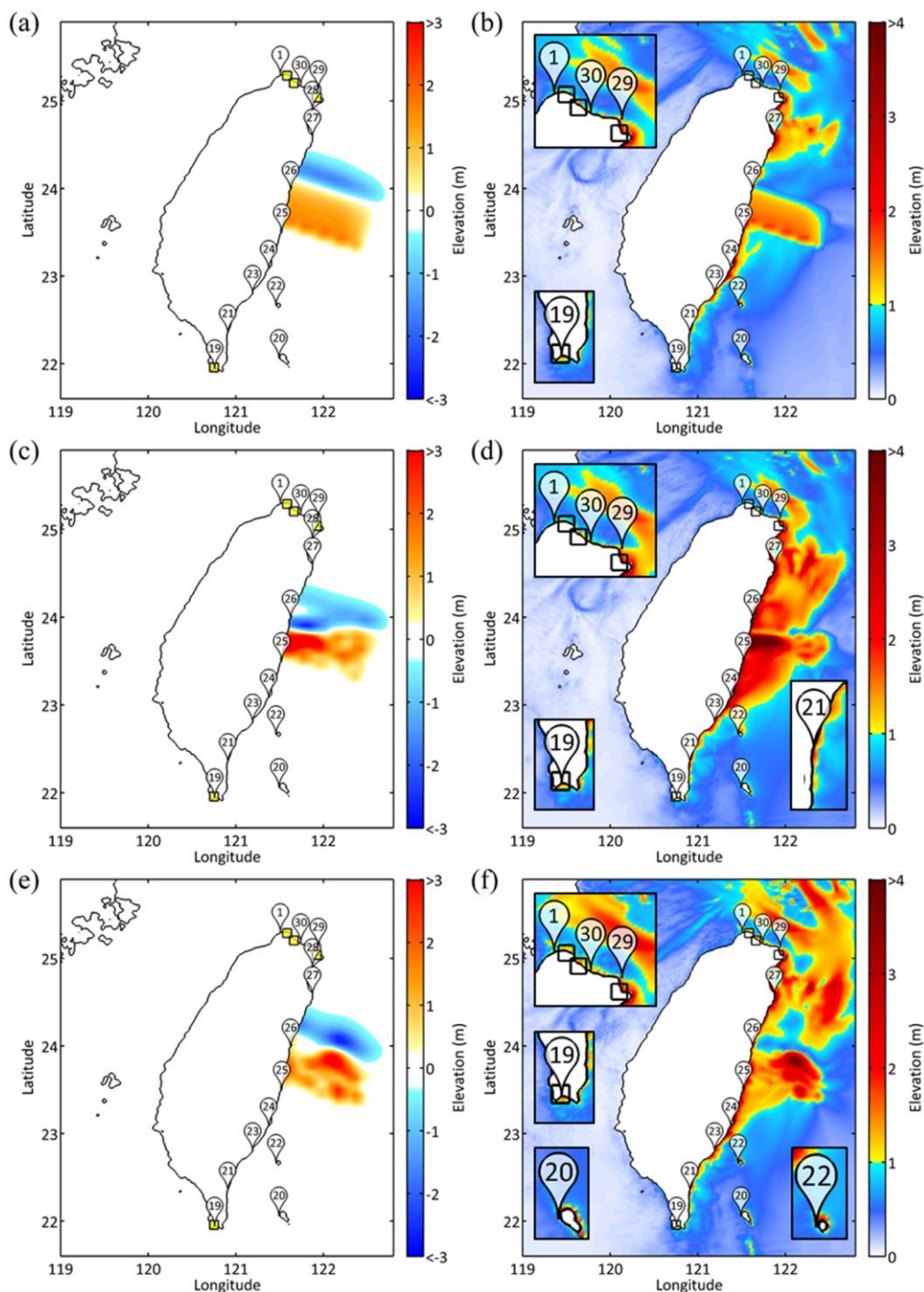
Fig. 3. The initial water elevation (a, c and e) and the distribution of energy propagation (b, d, and f). (a) and (b) displays the results from uniform slip distribution. (c) and (d) displays the results from Fig. 1b. (e) and (f) displays the results from Fig. 1d. In fundamental, seafloor dominants tsunami propagation, but the slip distribution has strong influence. In (a, c and e), yellow squares represent nuclear power plants; in (b, d and f), they are open squares.
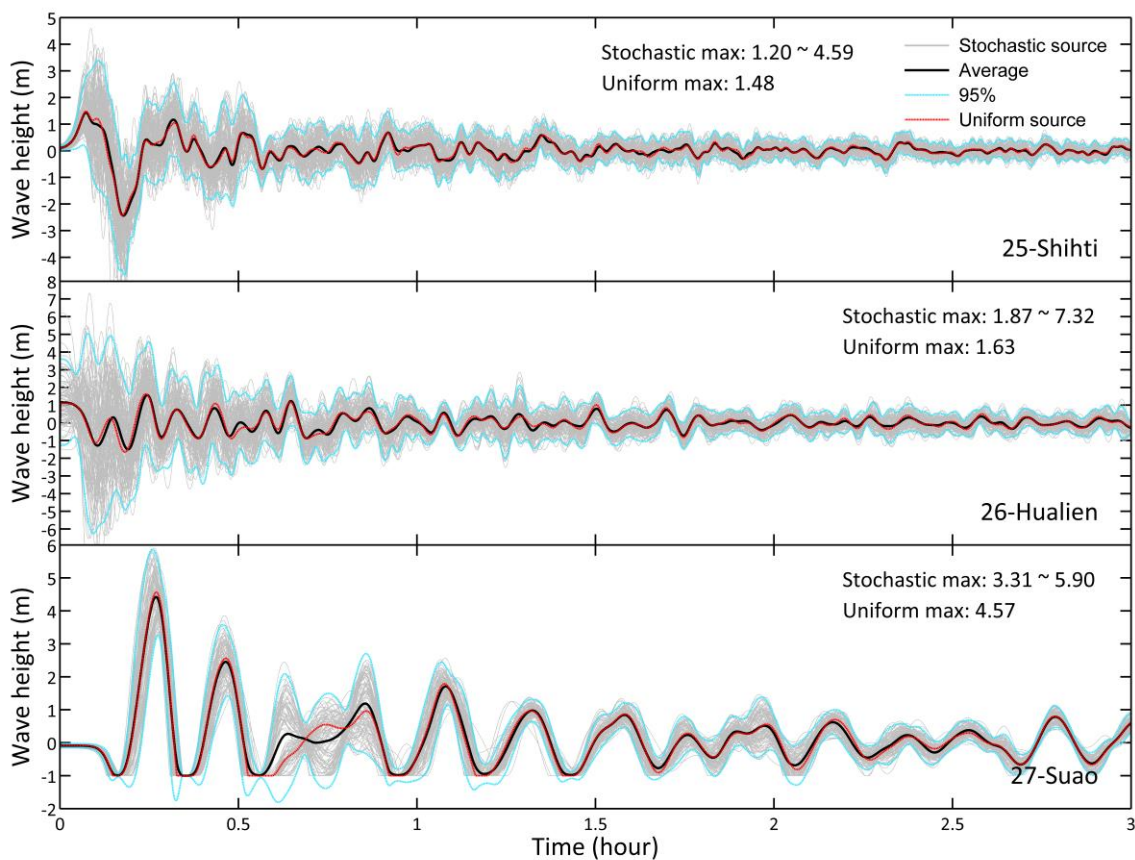
Fig. 4. The time series of wave heights recorded at station 25 (Shihti), 26 (Hualien) and 27 (Suao). Gray lines represent the time series of 100 different slip distributions; black lines represent the averages of the gray lines; blue lines represent the 95% confidence intervals; and red lines are the time series produced using uniform slip distributions. Parts of the wave heights on station 27 are lower than water depths, and these curves have been truncated.
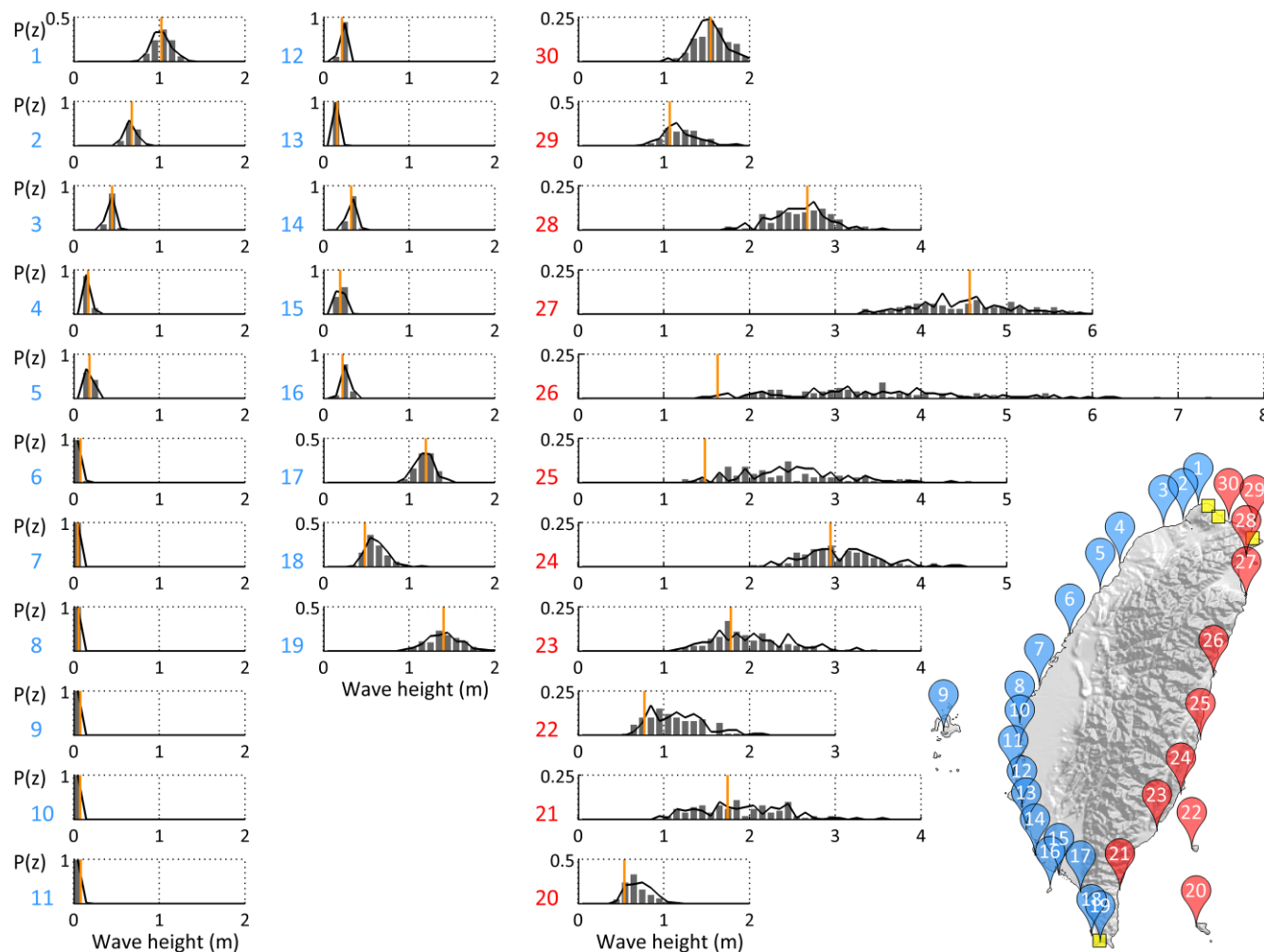
Fig. 5. The probabilities of PTA along the coast of Taiwan (blue: 1~19, red: 20~30). The histograms display the PTA derived from 100 different slip simulations. The black lines represent the results from another 100 simulations, and the orange lines represent the PTA obtained using a uniform slip distribution. The PTA probability distribution give a clear PTA range and its occurring probability.
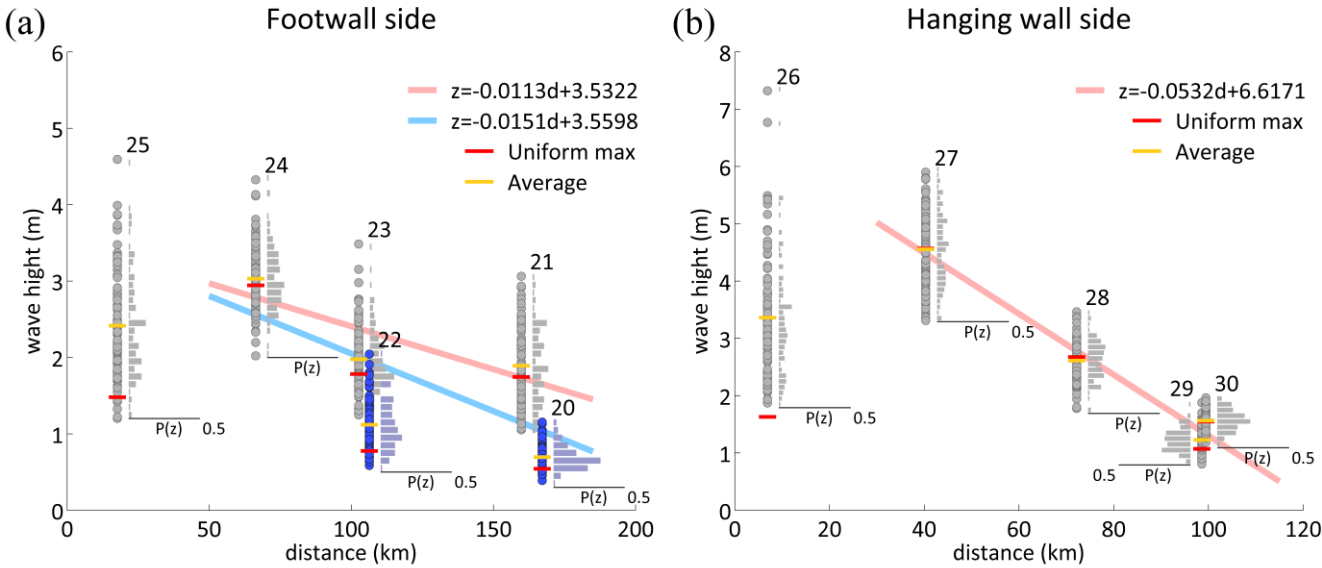
Fig. 6. The relation between distance and wave height for stations from 20 to 30 in the eastern Taiwan. (a) is the station on the footwall side. Station 20 and 22, blue color, are out of Taiwan island. Pink fitting line includes stations 21, 23 and 24. Blue fitting line includes stations 20 to 24. (b) is the stations on the hanging wall side. Pink fitting line includes stations 21 to 30. Both sides appear a linear decay and uncertainty range converging with distance increasing for tsunami amplitude. Red bars show the PTA of the uniform slip distribution and yellow bars show the average of the PTA from stochastic slip models.

Table 1. Statistical summary of PTA (all values in meters)

#	Station	Min	Max	σ	Average	Max (uni)
1	Linshanbi	0.80	1.32	0.108	1.04	1.02
2	Danshuei	0.55	0.83	0.061	0.68	0.68
3	Jhuwei	0.33	0.52	0.039	0.44	0.45
4	Hsinchu	0.13	0.24	0.025	0.17	0.17
5	Waipu	0.15	0.26	0.020	0.20	0.19
6	Taichung Port	0.07	0.11	0.009	0.08	0.08
7	Fanyuan	0.04	0.06	0.004	0.05	0.05
8	Bozihliao	0.05	0.07	0.004	0.06	0.06
9	Penghu	0.07	0.09	0.005	0.08	0.08
10	Dongshih	0.06	0.09	0.005	0.08	0.08
11	Jiangjyun	0.06	0.10	0.007	0.09	0.09
12	Anping	0.15	0.26	0.018	0.22	0.22

13	Yongan	0.11	0.20	0.016	0.16	0.16
14	Kaohsiung	0.23	0.43	0.039	0.33	0.33
15	Donggang	0.15	0.28	0.026	0.21	0.20
16	Siaoliouciou	0.17	0.40	0.046	0.26	0.22
17	Jiahe	0.90	1.44	0.098	1.19	1.20
18	Syunguangzuei	0.33	0.96	0.124	0.61	0.49
19	Houbihu	0.90	1.96	0.197	1.41	1.40
20	Lanyu	0.39	1.15	0.155	0.69	0.54
21	Dawu	1.05	3.06	0.487	1.89	1.74
22	Lyudao	0.58	2.04	0.316	1.12	0.78
23	Fugang	1.25	3.48	0.409	1.98	1.78
24	Chenggong	2.02	4.33	0.416	3.03	2.94
25	Shihti	1.20	4.59	0.680	2.42	1.48
26	Hualien	1.87	7.32	1.024	3.36	1.63
27	Suao	3.31	5.90	0.641	4.55	4.57
28	Gengfang	1.78	3.47	0.337	2.61	2.67
29	Longdong	0.80	1.88	0.202	1.23	1.07
30	Keelung	1.19	1.96	0.183	1.57	1.55

This table lists the maximum, minimum, standard deviation and average wave heights for the PTA probability distributions.

It also lists the maximum wave heights from uniform slip model.